Biomaterials 232 (2020) 119710

Contents lists available at ScienceDirect

Biomaterials

journal homepage: www.elsevier.com/locate/biomaterials

# Endothelialized collagen based pseudo-islets enables tuneable subcutaneous diabetes therapy

Alexander E. Vlahos[a], Sean M. Kinney[a,b,1], Benjamin R. Kingston[a,1], Sara Keshavjee[a], So-Yoon Won[a], Anastasiya Martyts[a], Warren C.W. Chan[a,b,c], Michael V. Sefton[a,b,*]

[a] Institute of Biomaterial and Biomedical Engineering, University of Toronto, Toronto, M5S 3G9, Canada
[b] Department of Chemical Engineering and Applied Chemistry, University of Toronto, Toronto, Ontario, M5S 3G9, Canada
[c] Department of Material Science and Engineering, University of Toronto, University of Toronto, Ontario, M5S 3G9, Canada

ARTICLE INFO

*Keywords:*
Pseudo-islets
Subcutaneous islet transplantation
Endothelialized collagen scaffold
Diabetes
Vascularization
CLARITY
Modular tissue engineering

ABSTRACT

Pancreatic islets are fragile cell clusters and many isolated islets are not suitable for transplantation. Furthermore, following transplantation, islets will experience a state of hypoxia and poor nutrient diffusion before revascularization, which is detrimental to islet survival; this is affected by islet size and health. Here we engineered tuneable size-controlled pseudo-islets created by dispersing de-aggregated islets in an endothelialized collagen scaffold. This supported subcutaneous engraftment, which returned streptozotocin-induced diabetic mice to normoglycemia. Whole-implant imaging after tissue clearing demonstrated pseudo-islets regenerated their vascular architecture and insulin-secreting β-cells were within 5 μm of a perfusable vessel – a feature unique to this approach. By using an endothelialized collagen scaffold, this work highlights a novel "bottom-up" approach to islet engineering that provides control over the size and composition of the constructs, while enabling the critical ability to revascularize and engraft when transplanted into the clinically useful subcutaneous space.

## 1. Introduction

Type I diabetes is caused by the destruction of the insulin-producing β-cells found within the pancreas [1]. The transplantation of pancreatic islets into the portal vein (i.e. the Edmonton Protocol) is one of the only approaches for achieving insulin independence [2]. Since many islets fail to engraft due to the instant blood mediated inflammatory response [3] and a lack of revascularization, multiple donors are required to achieve insulin independence [4]. The subcutaneous space is being pursued as an alternative transplantation site due to its accessibility, its ability to support a large transplant volume, and it being less invasive than the liver [5,6]. However, strategies such as a scaffold must be deployed to increase the vascularity or reduce in vivo fragmentation for pancreatic islets to survive the otherwise avascular space [6–9]. Without these strategies, pancreatic islets do not survive subcutaneous transplantation [6,9].

Following transplantation, pancreatic islets must become revascularized or they will experience a prolonged state of hypoxia and poor nutrient diffusion [10], detrimental to their survival and function [11]. This is particularly important when transplanting larger pancreatic islets (>150 μm diameter), which are more susceptible to forming a hypoxic-inner core [12,13]. Transplanting only smaller pancreatic islets is not feasible since pancreatic islets are highly variable in size (50–400 μm diameter) and there is a limited amount of donor tissue available. Furthermore, many donated islets are often unsuitable for transplantation due to fragmentation or poor quality caused by the isolation process [14].

To minimize the development of a hypoxic core, human and rat pancreatic islets have been digested and formed into size-controlled pseudo-islets using a variety of methods (reviewed in Ref. [15]). Pseudo-islets are an alternative "micro-tissue" [16] for pancreatic islet transplantation (within the kidney capsule in most cases [17,18]); however, they do not function when transplanted into the avascular subcutaneous space [19].

We have returned to this concept and created an all-in-one pseudo-islet by providing an endothelialized collagen scaffold (collagen gel seeded with endothelial cells) to generate a vascularized subcutaneous site with pseudo-islet engraftment (Fig. 1). The addition of an endothelialized collagen scaffold allowed us to manipulate the cell composition of the pseudo-islets formed from deaggregated islets (rat or

* Corresponding author. Institute of Biomaterial and Biomedical Engineering, University of Toronto, Toronto, M5S 3G9, Canada.
*E-mail address:* michael.sefton@utoronto.ca (M.V. Sefton).
[1] Authors contributed equally.

https://doi.org/10.1016/j.biomaterials.2019.119710
Received 7 October 2019; Received in revised form 13 December 2019; Accepted 18 December 2019
Available online 26 December 2019
0142-9612/ 

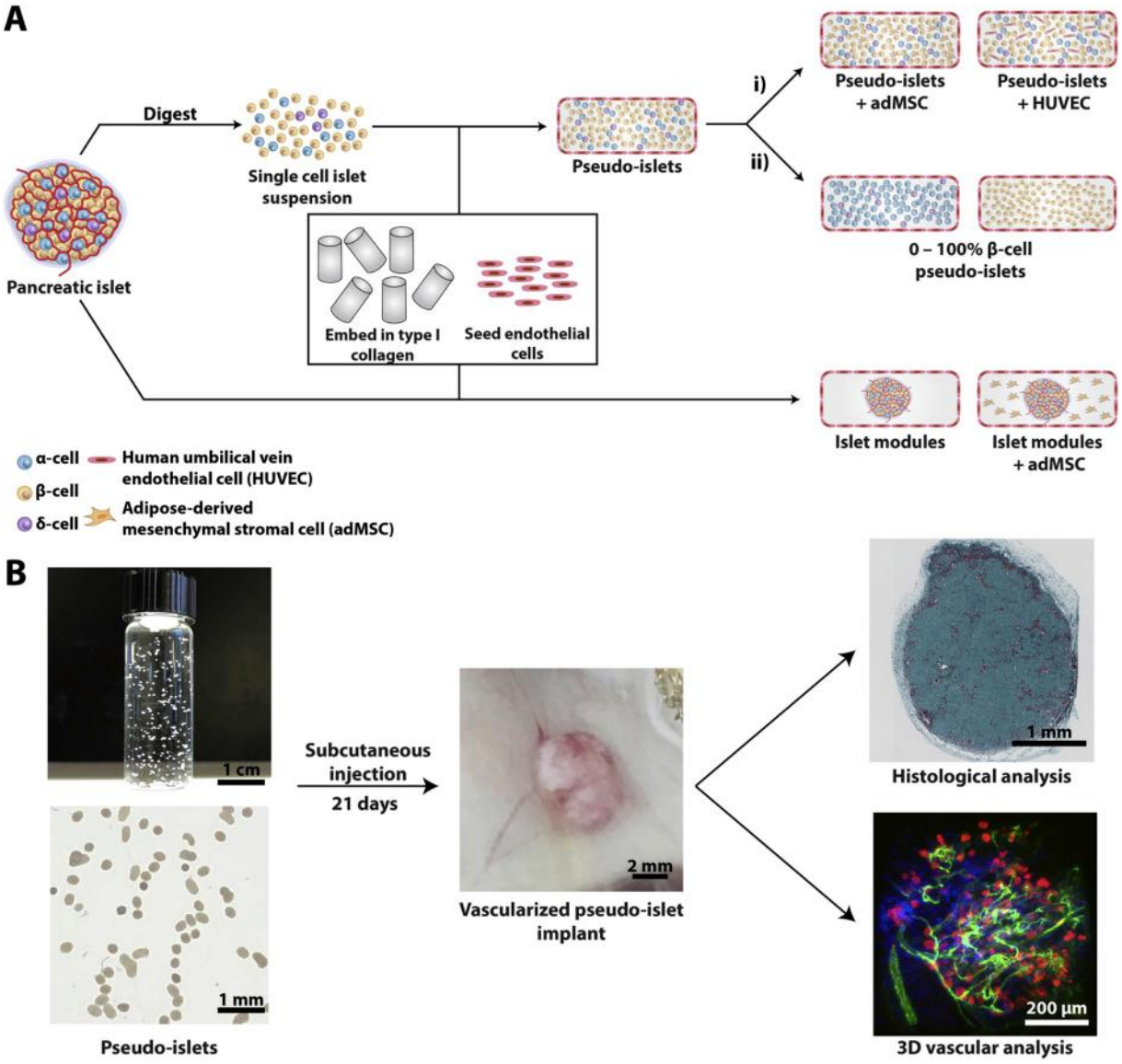


**Fig. 1.** Fabrication of tuneable pseudo-islets. Isolated pancreatic islets were digested into a single-cell suspension and then mixed with type I collagen. After being cut into sub-millimetre rods, pseudo-islets were seeded with Human umbilical vein endothelial cells (HUVEC) on the exterior. Pseudo-islets were fabricated with **i)** additional cells such as HUVEC or adipose-derived mesenchymal stromal cells (adMSC), **ii)** different mixtures of α and β-cells. Islet modules are native islets embedded within endothelialized collagen rods. **B)** Individual pseudo-islets are subcutaneously injected and self-assemble into a larger tissue organoid. Following 21 days, vascularized implants were removed and analyzed using histology and 3D imaging.

human) and add additional cell types reported to improve β-cell function such as adipose-derived mesenchymal stromal cells (adMSC) [20]. Our approach also allowed us to control the size of the pseudo-islet implants. Pseudo-islets were able to return diabetic SCID/bg animals to normoglycemia, unlike native islets and faster than islet modules (native islets in endothelialized collagen rods). The successful engraftment and therapeutic efficacy of these pseudo-islets was attributed to their revascularization and integration with the host's vasculature, which was confirmed by histology and large volume three-dimensional microscopy of the constructs after tissue clearing. This work highlights a novel "bottom-up" approach to islet engineering that provides control over the size and composition of the constructs, while enabling the ability to revascularize and engraft when transplanted into the subcutaneous space.

## 2. Materials and methods

### 2.1. Islet isolation

Primary rat islets were isolated from 12-week Wistar rats as previously described [6]. Briefly, the common bile duct was cannulated and perfused with collagenase solution (CIzyme, Vitacyte). Excised pancreases were incubated in a shaking water bath at 37 °C for 19 min before manual agitation. Following density purification using Histopaque 1100 (Sigma Aldrich), pancreatic islets were hand picked and islet equivalents (IEQ) were calculated based on volumetric assumptions [21]. Pancreatic islets were cultured in RPMI-1640 (Gibco) supplemented with 10% FBS (Gibco) and 1% PenStrep (Gibco). For in vivo and in vitro studies, multiple rat islet isolations were performed, with enough islets to span multiple test groups. Human islets were procured and shipped from the University of Alberta (IsletCore, Alberta Diabetes Institute); islets from two donors were used for this study (Supplementary Table 1).

### 2.2. Pseudo-islet fabrication

Rat or human pancreatic islets were digested using 0.25% Trypsin-EDTA (Gibco) for 5 min at 37 °C on an orbital shaker set to 120 rpm. Using supplemented RPMI-1640 media (10% FBS and 1% PenStrep), the trypsin was neutralized and a single cell suspension was created following vigorous pipetting. The viability of the islet cells was determined using LIVE/Dead™ Fixable near – IR Dead Cell Stain Kit (Invitrogen, Thermo Fisher Scientific) and was 90.7 ± 0.5% (average from 3 representative pseudo-islet fabrications).

Single islet cells were mixed with neutralized collagen (3.0 mg/mL – PureCol, Advanced Biomatrix) at 2 million islet cells/mL of collagen and drawn within polyethylene tubing (PE60, Intramedic). The collagen containing the islet cells were incubated at 37C for 1 h to allow the solution to gel and then cut using an automatic tube cutter to form individual microtissues [6,22]. The sub-millimetre collagen rods with embedded islet cells (pseudo-islets) were dynamically seeded with HUVEC (Lonza, 2 million cells/mL of collagen) for 1 h at 37 °C. Using this method, the number of pseudo-islets generated was approximately equal to the starting number of islet equivalents.

Pseudo-islets were cultured for up to 7 days in a 50:50 blend of supplemented RPMI-1640 and EGM-2 (Lonza). In some groups, pseudo-islets with additional HUVEC or adMSC (Lonza) embedded within the collagen (100 k cells/mL of collagen) were fabricated. For transplantation studies, pseudo-islets were cultured for 4 days before being transplanted. A list of pseudo-islet cell compositions is in Supplementary Table 2.

### 2.3. Pseudo-islet volume and sphericity

Pseudo-islets with and without adMSC were imaged at days 2, 4 and 7 using an AxioCam ICc1 camera (Zeiss). Pseudo-islet volume was calculated using the formula for an ellipsoid. Pseudo-islet sphericity was calculated using the following formula: $\text{Sphericity} = \frac{\text{Surface area of a sphere with an identical volume}}{\text{Surface area of a module}}$. Values of 1.0 indicated modules that remodelled into perfectly round spheres.

Islet cell sorting and single cell manipulation of pseudo-islet fabrication:

A single cell suspension of rat pancreatic islets was formed and stained using LIVE/Dead™ Fixable near – IR Dead Cell Stain Kit (Invitrogen, Thermo Fisher Scientific) and then re-suspended in FACS sorting buffer (PBS + 2.8 mM glucose + 1 mM EDTA + 25 mM HEPES + 1% BSA). β-cells ($A_{530}^{high}$) were sorted from the remaining islet cells ($A_{530}^{low}$) using the FACS Aria IIIU cell sorter (BD Biosciences). Pseudo-islets were fabricated using different combinations of sorted β-cells and α-cells. These pseudo-islets were cultured for 2 days, fixed using 4% PFA, and then stained overnight at 4 °C for insulin (1:400 dilution, Bioss Inc.), glucagon (1:200 dilution, Santa Cruz) and DAPI (1:400 dilution, Invitrogen). Following overnight incubation, samples were washed three times using PBST and then stained with a donkey anti-goat IgG antibody conjugated to alexa-647 (1:400 dilution, Thermo Fisher Scientific) for the anti-glucagon antibody. Samples were imaged using a Nikon A1 confocal microscope and processed using FIJI. Five individual pseudo-islets from each group over multiple isolations were used to quantify the proportion of $insulin^+$ and $glucagon^+$ cells using the 3D Objects Counter Analyzer in FIJI [23]. Percent compositions are given as an average ± SEM.

### 2.4. Confocal microscopy

Cultured pseudo-islets or native free islets were fixed using 4% paraformaldehyde (PFA, Sigma Aldrich) at days 2, 4 and 7. Samples were washed using PBST (PBS + 0.1% Tween-20) and then blocked using PBST supplemented with 2% bovine serum albumin (BSA, Sigma Aldrich). Following a 4-hr incubation in blocking solution, samples were stained overnight at 4 °C using antibodies against E-Cadherin, insulin, and glucagon. A complete list of antibodies and their dilutions is in Supplementary Table 3. Stained samples were imaged using a Nikon A1 confocal microscope and processed using FIJI.

### 2.5. Static glucose tolerance assay

Samples of 25 free islets or pseudo-islets were pre-incubated with low-glucose (3.3 mM) Krebs-Ringer Bicarbonate (KRB) buffer supplemented with 0.25% BSA for 40 min at 37 °C. Samples were then incubated in fresh low-glucose KRB buffer 1 h at 37 °C. After incubation, the samples were put into high-glucose (16.7 mM) KRB buffer for 1 h at 37 °C. Throughout the entire assay the samples were incubated on an orbital shaker (~50 RPM). Aliquots were taken after each of the incubation steps and stored at −20 °C. Samples were analyzed for rat insulin using a Rat/Mouse insulin ELISA kit (EZRMI-13K; EMD Millipore) according to the manufacturer's instructions. Insulin concentrations were presented as averages ± SEM. Insulin stimulation indices were calculated by taking the ratio of the insulin concentration in high glucose solution to the insulin concentration at low glucose solution, which was then averaged and reported ± SEM.

### 2.6. Islet perifusion assay

Perifusion assay was performed as previously described [24]. Briefly, samples of 125 native islets or pseudo-islets were loaded into perifusion chambers, which were stimulated using 16.7 mM glucose KRB. Secreted insulin was collected and measured by RIA (RI-13K, EMD Millipore). Secreted insulin was normalized to total insulin content of each sample to account for differences in islet size and β-cell number, as previously described [24].

### 2.7. Single cell $Ca^{2+}$ influx analysis

Pancreatic islets or pseudo-islets were cultured for 4 days and then washed 3 times with low-glucose KRB (3.3 mM). Samples were then incubated with Fluo-4 AM dye (2.5 μm, ThermoFisher Scientific) for 45 min, shaking at room temperature. Following incubation, samples were washed 3 times with low-glucose KRB and time-series images were captured using a Nikon A1 Confocal Microscope. Samples were imaged over a 5-min period (every 2 s) under fresh low-glucose KRB. Glucose was spiked into the chamber (25 mM glucose, final concentration) to minimize disruption of the islets or pseudo-islets, and then imaged for an additional 10-min period (every 2 s).

Cells stained positively with Fluo-4AM were manually selected on FIJI. From these cells, only cells that had a maximum fluorescence ($F_{max}$) that was 1.2-fold greater than the average basal fluorescence ($F_0$) were selected for subsequent analysis. As previously described [25], the relative fluorescence intensity at each time point was calculated using the formula: $F_r = \frac{F - F_0}{F_{max} - F_0}$.

### 2.8. Oxygen consumption rate analysis

The oxygen consumption rate (OCR) of native islets, and pseudo-islets with and without adMSC were measured using the Seahorse Xe24 instrument (Agilent, Santa Clara, CA) according to manufactures instructions. Briefly, 30 pseudo-islets with or without adMSC, or native free islets were loaded into the Xe24 capture plates (Agilent) and incubated in low glucose KRB buffer (2.8 mM glucose) for at least 1 h prior to running the assay. Xe24 injection cartridges were used to deliver glucose (16.7 mM final concentration) and different electron chain modulators (i.e. 5 μm oligomycin, 4 μm FCCP with 10 mM methyl pyruvate, and 5 μm antimycin and 5 μm rotenone) during the assay. Following each injection, samples were mixed and the OCR was sampled.

Following completion of the OCR assay, the total double-stranded DNA (dsDNA) content was isolated using a DNeasy Blood and Tissue Kit (Qiagen) and quantified using a Quant-IT™ PicoGreen™ dsDNA Assay kit (Thermo Fisher Scientific). The basal and maximal respiration rates for each sample were normalized to the total dsDNA of each sample.

### 2.9. Pseudo-islet transplantation

All animal experiments and surgeries were performed at the University of Toronto and were approved by the Faculty of Medicine Animal Care committee. SCID/bg mice (5–6 weeks; Charles River) were made diabetic using a single intraperitoneal injection (i.p.) of streptozotocin (180 mg/kg; Sigma-Aldrich) one week before transplantation. Non-fasting blood glucose was measured daily (OneTouch UltraStar2) and animals that showed at least two consecutive readings above 20 mM glucose were used for transplantation studies.

Pseudo-islets ($1.5 \times 10^6$ islet cells (~750 IEQ)) were washed with PBS before being subcutaneously injected using an 18-G needle, as previously described [6]. Animals were housed individually and non-fasting blood glucose levels were monitored daily for the first 21 days. In some transplants, animals were monitored three times a week for days 21–42. At days 7 and 14, animals were fasted for 4 h and then an intraperitoneal glucose tolerance test (IPGTT) was administered. Mice that returned to normoglycemia by day 21 were anaesthetized and the pseudo-islets were retrieved without sacrificing the animal. Non-fasting blood glucose levels were monitored for 2–3 days to confirm the pseudo-islets were responsible for the return to normoglycemia. Explants were sent for histological processing or processed using CLARITY.

### 2.10. Histological analysis

Explanted grafts were fixed in 4% paraformaldehyde (Sigma) for 48 h prior to histological processing by the Pathology Research Laboratory at the Toronto General Hospital. Implants were sectioned at multiple levels, 100 μm apart and stained using Masson's Trichrome, H &E, CD31, SMA and Insulin. Sections were imaged and scanned (20X, Aperio ScanScope XI; Leica Microsystems) at the Advanced Optical Microscopy Facility at the University of Toronto. Scans were then analyzed using ImageScope software version 11 (Aperio). A complete list of antibodies used in this study can be found in Supplementary Table 3.

### 2.11. CLARITY processing and imaging

Animals were injected with GSL-1 lectin (Vector laboratories) conjugated to alexa-555 (Thermo Fisher Scientific) via the tail vein prior to whole-body perfusion with PBS + 10 U/mL Heparin and 0.5% sodium nitrate, and monomer solution (PBS + 2% acrylamide and 4% formaldehyde). Clearing was performed as previously described [6,26] and clarified implants were stained using an anti-insulin antibody (1:400, Dako) at room temperature. Following one week of staining, implants were washed three times using PBS +0.1% Triton X and then incubated with a goat anti-guinea pig antibody conjugated to alexa-647 (1:1000, Thermo Fisher Scientific). Clarified tissues were then incubated in Refractive Index Matching Solution (RIMS) [27] to match the refractive index and then imaged using light-sheet microscopy (SickKids Toronto).

### 2.12. CLARITY image analysis

Three-dimensional (3D) images generated through light-sheet imaging were processed and analyzed to quantify vessel and insulin positive cell characteristics of the implants using custom MATLAB scripts and the segmentation tool Ilastik [28]. Blood vessels and cell nuclei were segmented and quantified using a multistep process outlined in Supplementary Fig. 1. First, a pre-processing MATLAB algorithm was applied to the blood vessel and nuclei channels to normalize local and global variations in signal intensity across the image volume. Second, a machine learning-based tool, Ilastik [28], was trained to segment blood vessel and nuclei from the pre-processed images to create binary blood vessel and nuclei images. Third, the Ilastik segmented blood vessel and nuclei images underwent a post processing MATLAB algorithm to remove artifacts specific to each feature. For blood vessels, the edges of the tissue were removed due to the presence of auto fluorescent false positive signal at the tissue edges and the result was the final segmented blood vessel network. For nuclei, the tissue edges and small artifacts were removed and merged nuclei were separated using a seeded watershed algorithm resulting in the final segmented nuclei image. The segmented nuclei and blood vessel images were then used to quantify features of the implants using an automated MATLAB script. An Euclidean distance transformation was applied to the segmented vessel channel to map the diameter of the blood vessels and the distance of the segmented nuclei from the nearest vessel. Insulin positive cells were identified by overlaying the insulin channel with the segmented nuclei and calculating the mean insulin intensity per nuclei, a manual threshold was then used to classify cells as insulin positive or negative. The characteristics from this analysis was output as numerical measurements, and as images for visualization of the vessel networks and insulin positive cells using IMARIS 8.1. All code used in this paper is available on Github (http://github.com/BenKingston/Islet_analysis_Vlahos), or from the developers of Ilastik (https://www.ilastik.org, or https://github.com/ilastik).

### 2.13. Statistical analysis

A one-way ANOVA with a Games-Howell post hoc test [29] was used to compare the means among different experimental groups unless otherwise stated in the results or figure captions. In the event that the data was not normally distributed (Shapiro-Wilk test), then a Kruskal-Wallis with Dunn's correction for multiple comparisons or a Mann-Whitney *U* test was used to test for significance. Data were considered statistically significant at a p value of 0.05. Data are presented as average ± SEM, unless otherwise stated. All statistical analysis was performed using SPSS software version 22 (IBM).

### 2.14. Data availability

The datasets generated during and/or analyzed during the current study are available from the corresponding author on reasonable request.

## 3. Results

### 3.1. Islets were deaggregated and reconstituted to form functional pseudo-islets

We first evaluated pseudo-islets fabricated with customized cellular compositions using deaggregated islet cells and controlled additions of adMSC and HUVEC in vitro. These additional HUVEC or adMSC were mixed with deaggregated islet cells to form the different pseudo-islet groups (outlined in Supplementary Table 2). Collagen was quickly mixed to minimize the time islet cells spent as a single cell suspension during fabrication, thus limiting β-cell death due to ECM detachment (anoikis) [30]. Pseudo-islets were designed so that each individual construct would contain approximately 2000 islet cells – corresponding to the approximate number of islet cells found within a single islet equivalent unit (IEQ) [31,32] as well as a coating of HUVEC on the exterior. This allowed us to compare pseudo-islets with native islets and islet modules (native islets embedded within endothelialized collagen) at equivalent doses (Fig. 1).

Unlike native rat islets, in which insulin and glucagon positive cells

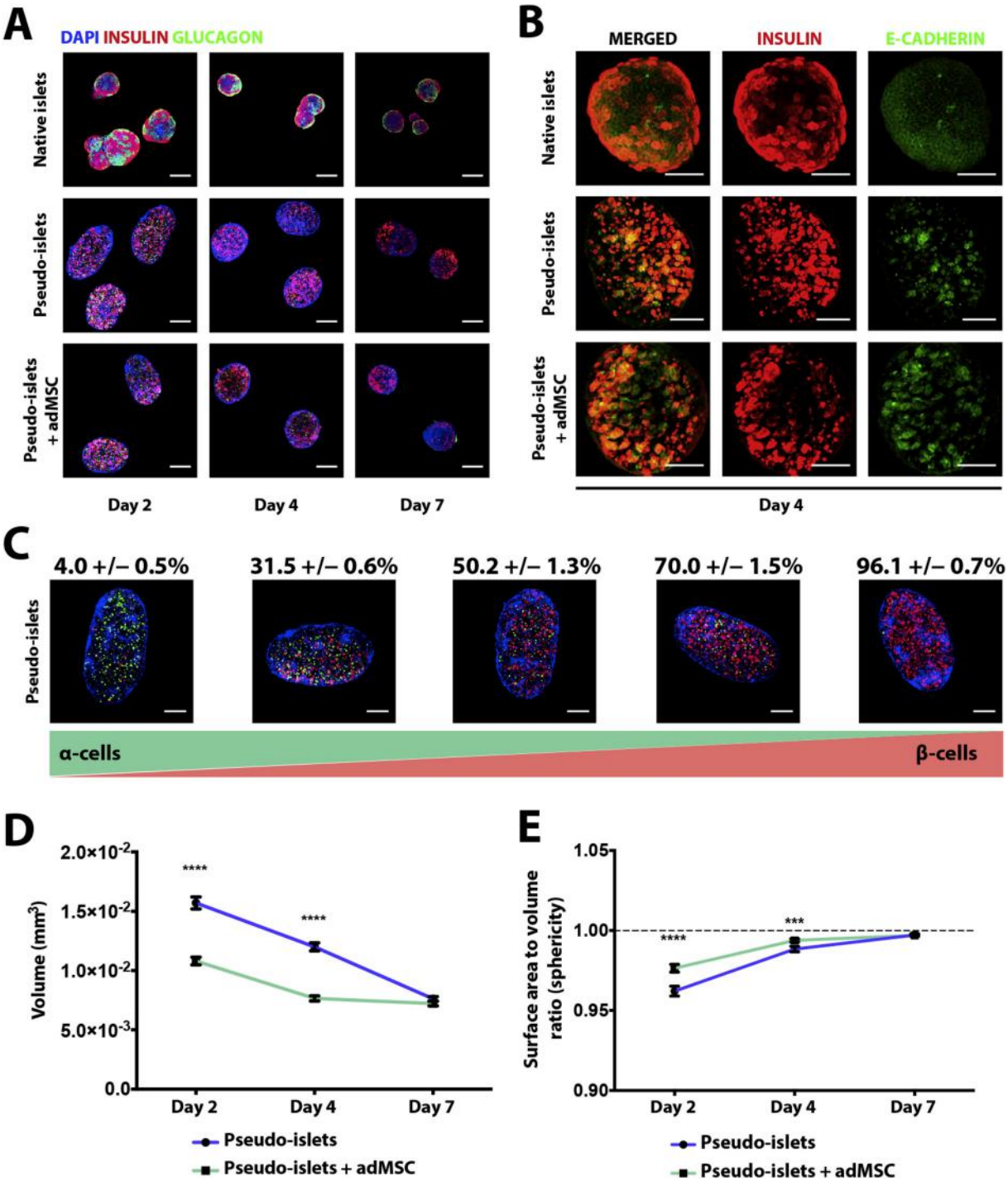


**Fig. 2. In-vitro manipulation of pseudo-islets. A)** Native islets and pseudo-islets with and without adMSC contained insulin$^+$ (red) and glucagon$^+$ (green) cells at days 2, 4 and 7. **B)** Native islets and pseudo-islets, with and without adMSC, stained for insulin (red) and E-cadherin (green) at day 4. E-cadherin was found on the membrane of insulin$^+$ cells of the native islets and pseudo-islets with and without adMSC. **C)** Pseudo-islets fabricated with different mixtures of β-cells (insulin$^+$, red) and α-cells (glucagon$^+$, green). The percentage of β-cells for the different pseudo-islet groups was quantified from the maximum intensity projections (n = 5 for each group, ± SEM). The remaining percentage of cells for each group was comprised of α-cells and other non-β-cell islet cells. Individual channels for the respective photos can be found in Supplementary Fig. 4. **D)** Pseudo-islets + adMSC were significantly smaller at days 2 and 4 ($p < 0.001$, Mann-Whitney *U* test) compared to pseudo-islet without adMSC. By day 7, both groups were comparable in size. n ≥ 34 for pseudo-islets at all time points. n ≥ 50 for pseudo-islets + adMSC at all time points. **E)** In addition to becoming smaller, pseudo-islets with and without adMSC became more spherical over time. The addition of adMSC caused pseudo-islets to be more spherical at days 2 ($p < 0.001$, Mann-Whitney *U* test) and 4 ($p < 0.005$, Mann-Whitney *U* test) but this difference was not present at day 7. Scale bars = 200 μm ***$p < 0.005$, ****$p < 0.001$. (For interpretation of the references to colour in this figure legend, the reader is referred to the Web version of this article.)

were arranged in a specific cyto-architecture [33] (Fig. 2A, **top row, red and green cells**), cells were randomly distributed in all pseudo-islet groups, with or without adMSC (Fig. 2A, **middle and bottom row**). E-cadherin expression appeared uniformly throughout all of the cells in the native islet, with a greater expression found on the membranes of insulin$^+$ cells (Fig. 2B, **green stain**). The expression of E-cadherin (green stain) in the two pseudo-islet groups was found to be predominately on insulin$^+$ cells (red stain), many of which had formed smaller aggregates on the interior (Fig. 2B). This was important since E-cadherin expression has been reported to correlate with the insulin secretion ability of β-cells [34]. Pseudo-islets fabricated using human islets showed a comparable distribution of islet cells (Supplementary Fig. 2A) with E-cadherin$^+$ expression (Supplementary Fig. 2B) similar to rat pseudo-islets.

To illustrate the cellular tuneability of this approach, we created a series of pseudo-islet constructs with the same number of total islet cells, but varying amounts of α- and β-cells (Fig. 2C). β-cells were sorted from a single cell suspension of rat islet cells using flavin adenine dinucleotide (FAD) autofluorescence [35] (91.9 ± 0.8% purity of single cell population – Supplementary Fig. 3). The ability to manipulate the cell composition of the pseudo-islets is shown by differences in the proportion of stained α (glucagon$^+$, green cells) and β-cells (insulin$^+$, red cells) within the different pseudo-islets (Supplementary Fig. 4). This demonstrates the tuneability of these constructs.

Pseudo-islet size is another factor we can control during fabrication to yield transplant tissues with defined sizes - something not possible with native islets (Supplementary Fig. 5B). The endothelialized collagen scaffold contracts and remodels, so that pseudo-islets became more spherical over time when cultured (Fig. 2D and E and Supplementary Fig. 5A). We found that the inclusion of adMSC resulted in more prominent remodelling; allowing us to tune the size to significantly smaller and more spherical pseudo-islets at days 2 and 4, post fabrication (Fig. 2D, E, $p < 0.001$). By day 7, however, there was no significant difference in the volume between the pseudo-islets with or without adMSC.

We next evaluated the function of the pseudo-islet constructs in vitro to ensure that their function was similar to native islets. Pseudo-islets remained glucose sensitive when pseudo-islets and native islets were challenged with glucose under perifusion (Fig. 3A). Under basal conditions, the insulin secretion of pseudo-islets was significantly lower than the native islet controls (Fig. 3B, $p < 0.05$), but after stimulation with glucose (16.7 mM), both pseudo-islets and native islets responded with increased insulin secretion (Fig. 3A – 1st phase). Pseudo-islets had a delayed 1st phase insulin secretion response (initial burst; 10 min), however this difference was not significant relative to native islets (Fig. 3B – 1st phase). In addition, the 2nd phase insulin secretion profiles (sustained release) were comparable between pseudo-islets and native islets (Fig. 3B). Another metric of insulin secretion dynamics is the influx of $Ca^{2+}$ into β-cells in response to a glucose stimulus, which signals insulin secretion [25]. $Ca^{2+}$ influx of pseudo-islets and native islets was found to be comparable between native islets and pseudo-islets (Fig. 3C), although not all cells responded (Supplementary Fig. 6, Supplementary Videos #1 and #2).

Supplementary video related to this article can be found at https://doi.org/10.1016/j.biomaterials.2019.119710

At days 4 and 7 (post-fabrication), pseudo-islet groups secreted less insulin under low glucose static conditions than native islets, although this difference was only statistically significant at day 7 (Fig. 3E, $p < 0.05$). Under high glucose conditions (16.7 mM), pseudo-islets secreted a greater amount of insulin compared to native islets on day 4 (Fig. 3D, $p < 0.05$), but not at day 7 (Fig. 3E). Due to lower basal rates, insulin stimulation indices were significantly greater for pseudo-islets compared to native islets (Supplementary Fig. 7). The presence of adMSC caused pseudo-islets to secrete a significantly greater amount of insulin when stimulated compared to pseudo-islets without adMSC and native islets (Fig. 3D, $p < 0.05$); this difference was not observed at day 7 (Fig. 3E).

We next assayed the mitochondrial health of the pseudo-islet constructs. Islet mitochondrial health (i.e. respiration potential, measured by oxygen consumption rate (OCR)) is important for the insulin-secretion activity of islets [36], and is a predictor of transplant success [37]. Under basal glucose conditions (3.3 mM), pseudo-islets with or without adMSC had a lower OCR than native islets at day 4 (Supplementary Fig. 8B). However, in response to glucose stimulation (16.7 mM), the change in OCR of pseudo-islets with or without adMSC was comparable to native islets (Supplementary Figs. 8A and D). In addition, the maximal respiration potential of the pseudo-islets was similar to native islets (Supplementary Fig. 8C). These results suggested that pseudo-islets had comparable metabolic activity to native islets in response to high glucose.

### 3.2. Subcutaneously transplanted pseudo-islets returned diabetic SCID/bg to normoglycemia

We then tested the pseudo-islet constructs relative to islet modules and free islet when transplanted into a rodent model of hyperglycemia. Pseudo-islets were cultured for 4 days prior to subcutaneous transplantation to allow the constructs to remodel to a comparable size and sphericity to native islets, but with less variation (Supplementary Fig. 5C). An equivalent dose ($1.5 \times 10^6$ islet cells (~750 IEQ)) of pseudo-islets, islet modules [native islets in endothelialized collagen gel rods], or free islets alone were subcutaneously transplanted into streptozotocin-induced diabetic mice (SCID/bg). Free islet transplants were unable to return any diabetic recipients to normoglycemia within 21 days (red line – Fig. 4A and B), due to the inability to effectively vascularize native islets without a scaffold in the subcutaneous space [6,8,9]. On the other hand, STZ-induced diabetic SCID/bg mice returned to normoglycemia (<11.1 mM) regardless of whether they were subcutaneously transplanted with pseudo-islets (6 of 9 animals, Fig. 4A and B – blue solid line) or with native islet module controls (2 of 3 animals, Fig. 4A and B – blue dotted line). However, pseudo-islets showed a faster return to normoglycemia compared to the islet module controls (Fig. 4B, ~10 days vs. 16 days). Animals that returned to normoglycemia had their grafts retrieved, resulting in a rapid return to hyperglycemia (Fig. 4A), indicating the effect was due to the implants themselves.

At day 14, animals were administered an intraperitoneal glucose tolerance test (IPGTT) to assess the graft's ability to respond to a bolus of glucose (Fig. 4C). Animals transplanted with pseudo-islets were able to resolve the glucose bolus and return animals to normoglycemia, comparable to the non-diabetic controls (Fig. 4C). Islet module controls responded partially to the glucose bolus, and some of the animals returned to normoglycemia within 120 min (Fig. 4C – dotted blue line). Animals transplanted with free islets were unable to resolve the glucose bolus (Fig. 4C – red line). An AUC analysis of the blood glucose readings confirmed the significant differences between animals transplanted with free islets and pseudo-islets (Fig. 4D, $p < 0.005$). Islet modules and pseudo-islets did not have any significant differences between the two groups. These results show that the endothelialized collagen pseudo-islet constructs were able to have a similar therapeutic effect as the islet module constructs.

Additionally, HUVEC and adMSC were embedded within pseudo-islets with the aim of improving vascularity [16] and islet function [20,38] when subcutaneously transplanted. Pseudo-islets with embedded cells (adMSC or HUVEC) had comparable therapeutic efficacies to pseudo-islets alone (Supplementary Fig. 9). Interestingly, the improved return to normoglycemia seen in pseudo-islets with adMSC was not seen in the native islet module + adMSC control group, where the inclusion of these cells had a detrimental effect on blood glucose regulation (Supplementary Fig. 10).

We then wanted to confirm the compatibility of this pseudo-islet method with human tissues. To do this, pseudo-islets were fabricated

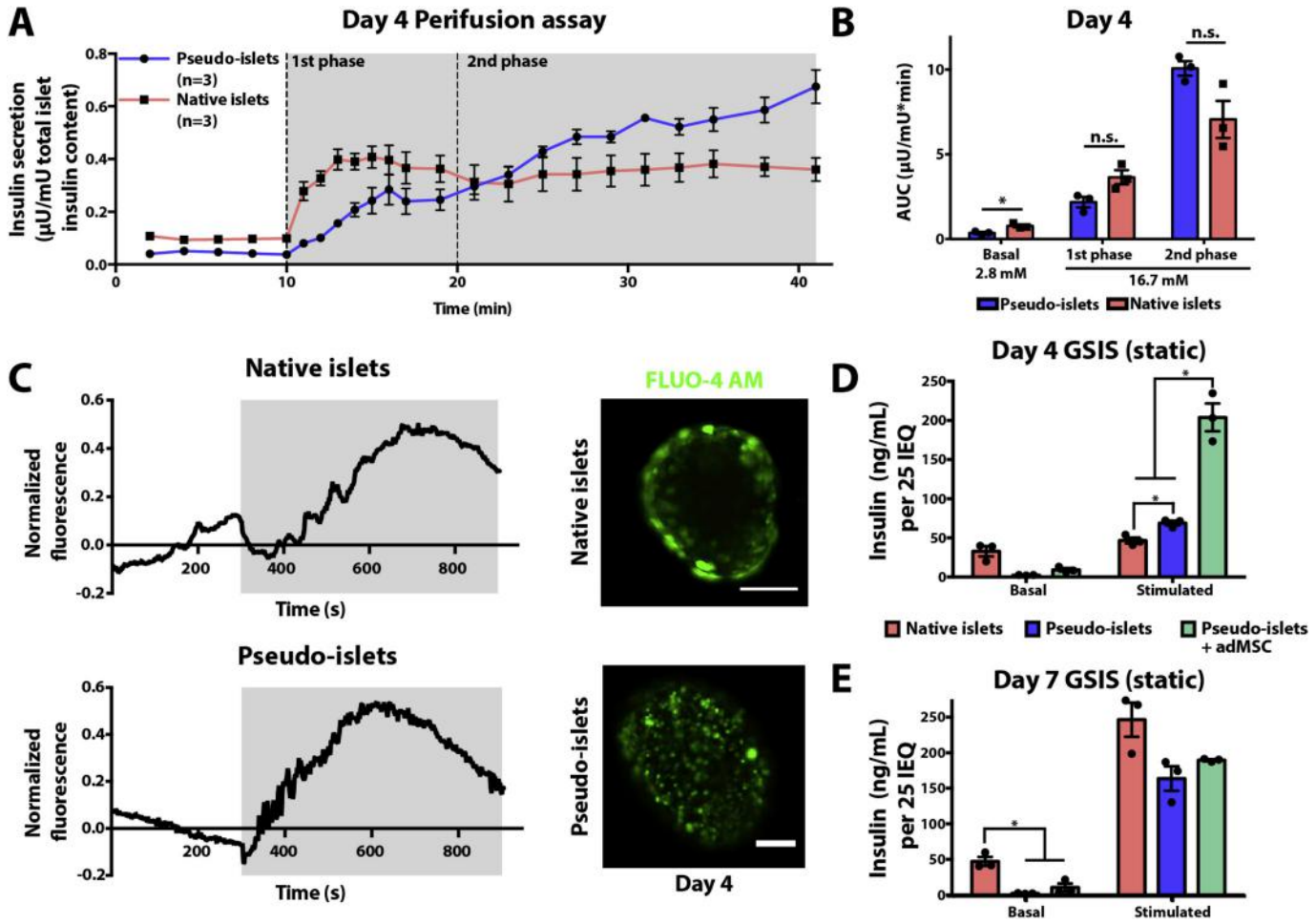


**Fig. 3. Pseudo-islets secrete insulin in response to glucose. A)** The insulin secretion activity of native islets and pseudo-islets was compared under dynamic flow conditions (n = 3 for all groups). Native islets secreted more insulin under basal glucose conditions (2.8 mM) compared to pseudo-islets. Following stimulation (16.7 mM glucose – **grey area**), pseudo-islets showed a comparable 1st phase (first 10 min) and 2nd phase insulin secretion response compared to native islets, **(B)** confirmed with an AUC analysis. **C)** Single-cell $Ca^{2+}$ signalling of responsive cells from native islets and pseudo-islets following stimulation with glucose at day 4 (n ≥ 12). Responsive cells from both groups showed increased fluorescence intensity over time following stimulation with glucose (25 mM – **grey area**). Representative maximum intensity projections of native and pseudo-islets; scale bars = 100 µm. **D)** A glucose stimulated insulin secretion (GSIS) assay was performed at days 4 and 7 under static conditions (n = 3 for all groups). At day 4, pseudo-islets with and without adMSC had a significantly greater amount of insulin secreted compared to the native islet control when stimulated with glucose (16.7 mM). The addition of adMSC to pseudo-islets resulted in a greater insulin secretion compared to pseudo-islets alone ($p < 0.05$). At day 7, native islets secreted a significantly greater amount of insulin during incubation in the basal glucose (3.3 mM) solution compared to the pseudo-islet groups, however there was no significant difference when stimulated. *$p < 0.05$.

using human islet cells with and without adMSC were subcutaneously transplanted. The pseudo-islet dose used here ($1.5 \times 10^6$ islet cells (~750 IEQ)) was sub-therapeutic due to rodents being less sensitive to human insulin [39] (Supplementary Figs. 11A and B), but explanted pseudo-islets were well vascularized ($CD31^+$ vessels) with insulin positive cells present throughout the implants (Supplementary Figs. 11C and D). These results highlight that this approach is capable of creating viable and vascularized transplants from human tissues, but a higher dose is required to achieve normoglycemia [39].

### 3.3. Subcutaneous vascularization of pseudo-islets

The next step was to determine how vascularized the pseudo-islets were in the otherwise avascular subcutaneous space. Histological analysis confirmed that all pseudo-islet implants were well vascularized ($CD31^+$) with mature ($SMA^+$) vessels at day 21 (Supplementary Fig. 12A). Native free islets could not be reliably explanted and assessed. The number of $CD31^+$ vessels was comparable between all of the pseudo-islet groups, regardless of the additional embedded HUVEC or adMSC (Supplementary Fig. 12B). Insulin positivity among the three groups was also not significantly different (Supplementary Fig. 12C). Grafts within each of the pseudo islet groups showed colocalization of a dense vasculature with insulin positive β-cells (Supplementary Fig. 12A – bottom panel).

To analyze large volumes of the implant vasculature we utilized tissue clearing, 3D optical microscopy and image analysis. Based on histological analysis, pseudo-islets were entirely vascularized by host-derived vessels at day 21 (Supplementary Fig. 13). Animals were injected with GSL-1 lectin conjugated to alexa-555 via the tail-vein to visualize the graft's integration with the host's vascular system in 3D (Fig. 5A, J **and** Supplementary Videos #3 and #4**)**. The average distance of a perfusable vessels to any of the cells ($DAPI^+$) within pseudo-islet or the native islet module controls was 35 ± 9.8 µm and 31.2 ± 5.1 µm, respectively (Fig. 5**I, R**) – well within the 150-µm diffusion limit of oxygen in tissues [40]. This confirmed that the pseudo-islets were well vascularized. The percent vessel volume ($GSL\text{-}1^+$ voxels per total voxels) of pseudo-islets and native islet modules was 8.0 ± 1.0% and 6.5 ± 0.6%, respectively (Fig. 5F, **O**), however pseudo-islets appeared to have a greater distribution of smaller diameter vessels throughout the graft (Fig. 5C). In comparison, islet module controls

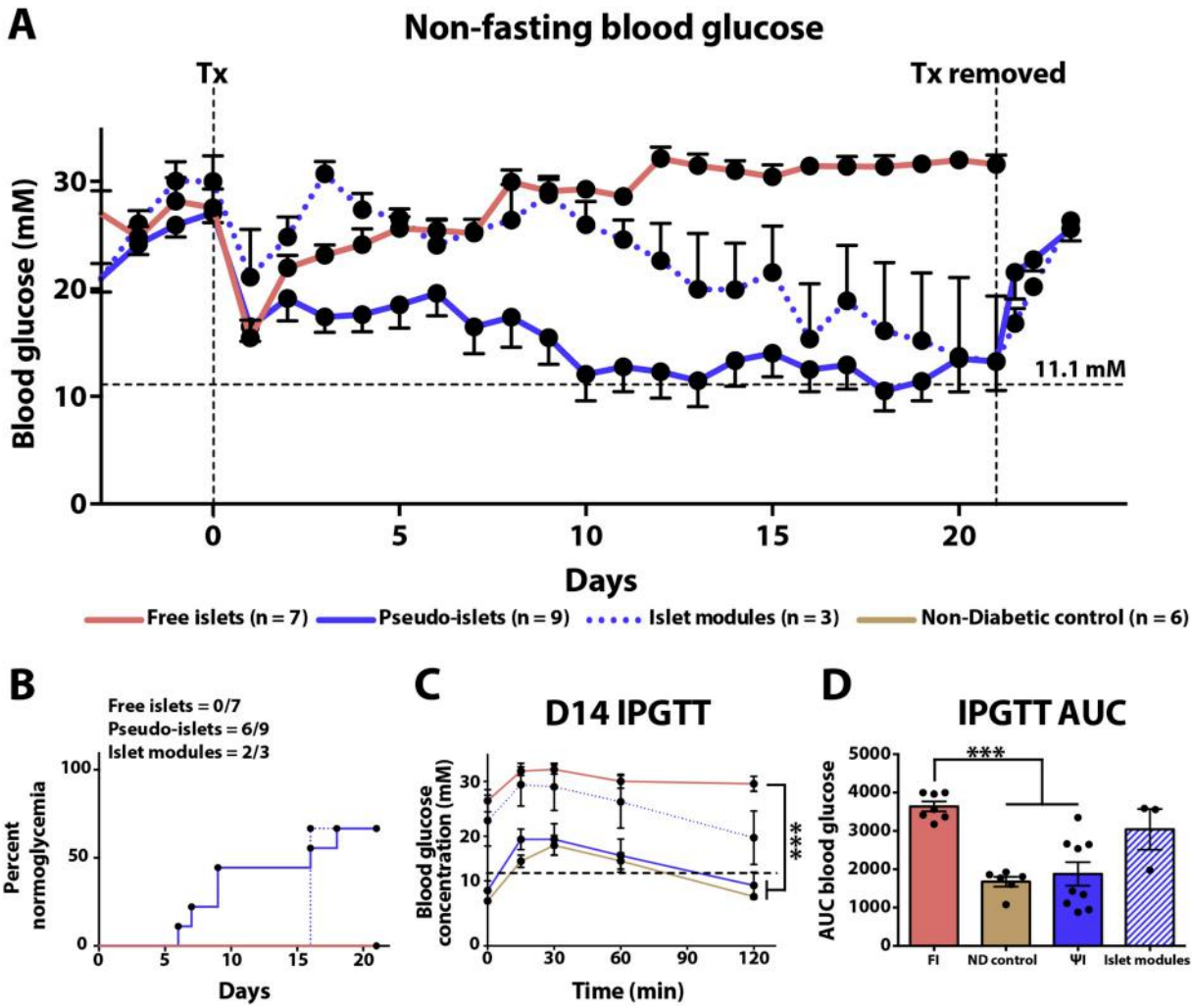


**Fig. 4. Pseudo-islets outperform islet modules when subcutaneously transplanted. A)** Average non-fasting blood glucose readings for animals transplanted with islet modules (islets embedded within endothelialized collagen, dotted blue line, n = 3) or pseudo-islets (ΨI, solid blue line, n = 9). Free islets without any endothelialized collagen scaffold (red line, n = 7) were also subcutaneously transplanted. At day 21, animals that had returned to normoglycemia had their implants removed without sacrificing the animal. Individual non-fasting blood glucose levels can be found in Supplementary Fig. 16. **B)** Kaplan-Meyer survival plot used to visualize when animals became normoglycemic. Mice transplanted with either pseudo-islets or islet modules returned to normoglycemia significantly faster than the native free islet control ($p = 0.009$ for ΨI; $p = 0.005$ for islet modules, log-rank, Mantel-Cox test). **C)** At day 14 an IPGTT was performed after animals were fasted and animals transplanted with pseudo-islets and islet modules were able to respond to the glucose bolus. Animals transplanted with pseudo-islets had a response to the glucose bolus comparable to that of the non-diabetic controls (n = 6). Repeated-measures ANOVA with a Games-Howell post hoc test revealed a significant difference between native free islets and the animals transplanted with pseudo-islets ($p = 0.001$). This significant difference was also as confirmed by an **D)** AUC analysis. (For interpretation of the references to colour in this figure legend, the reader is referred to the Web version of this article.)

appeared to have fewer vessels distributed throughout the graft, but had a greater number of larger diameter vessels (Fig. 5L).

Supplementary video related to this article can be found at doi:mmcdoino

In addition, whole-implants were stained with insulin to visualize β-cells (Fig. 5). The density of insulin$^+$ cells throughout pseudo-islet and islet module implants at day 21 was 1310 ± 153 insulin$^+$ cells/mm$^3$ and 2008 ± 448 insulin$^+$ cells/mm$^3$, respectively (Fig. 5H, **Q**). Both types of implants showed a close association between insulin$^+$ β-cells and the perfusable vasculature of the graft (Fig. 5I, R), and the above noted differences in vessel structures followed the different distributions of β-cells between the two different types of grafts (Fig. 5A, J). The average distance of a perfusable vessel to an insulin$^+$ cell was less than 5 μm (Fig. 5A, J **inlets, I, R**), in both pseudo-islet and islet module implants (4.9 ± 1.7 μm and 3.8 ± 0.3 μm). This confirmed that β-cells were closely associated with perfusable vessels in the implants even after being fabricated into pseudo-islets.

## 4. Discussion

### *4.1. Pseudo-islets are rationally designed to enable subcutaneous delivery*

The subcutaneous space is a promising alternative site for islet transplantation, however it is poorly vascularized [19]. Current strategies aim to overcome this problem and make this space compatible with islet transplantation by delivering pancreatic islets within biological scaffolds to drive revascularization and cell engraftment [6,8,9]. However, prior to islet revascularization, pancreatic islets are susceptible to apoptosis due to prolonged exposure to hypoxia and poor nutrient diffusion [10]. Since islet transplantation efficiency is also affected by islet size (even in the vascularized kidney capsule) [12], fabricating size-controlled pseudo-islets from deaggregated islets has been pursued as an alternative [17,41]. These pseudo-islets were functionally comparable to native islets in vitro [17], but many current pseudo-islet constructs only function when transplanted into the kidney capsule [17,18,42] and would not be expected to survive

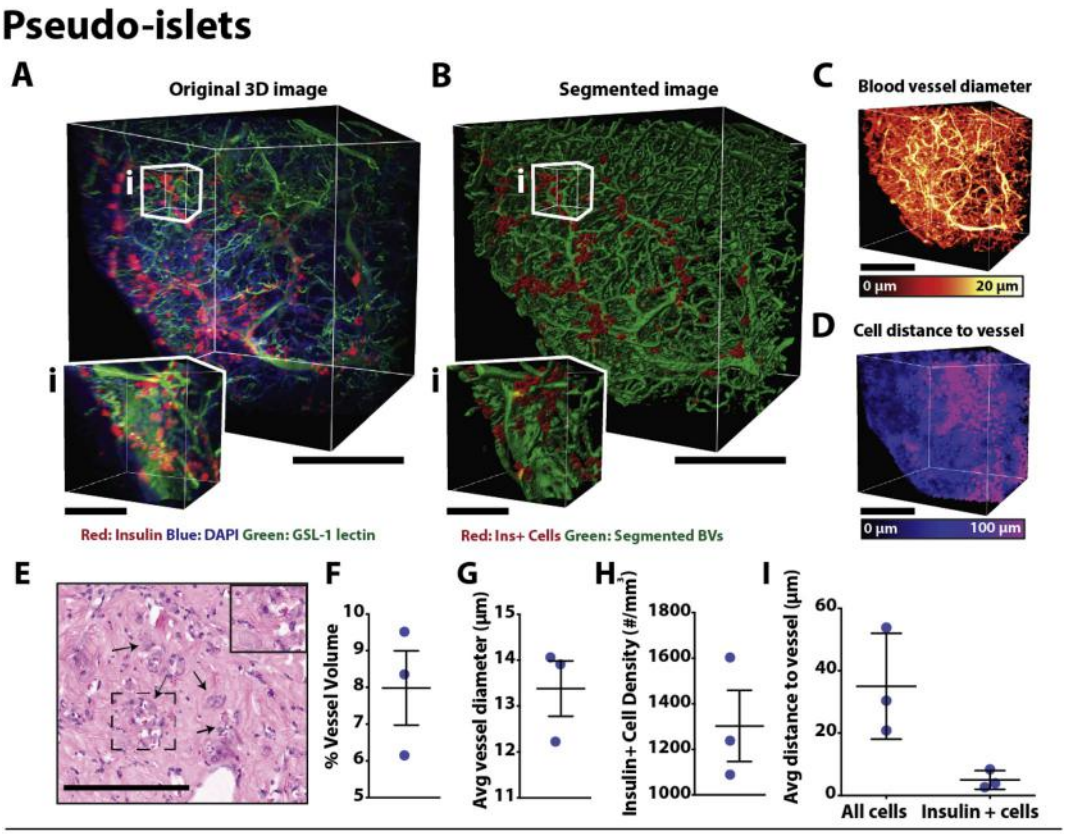


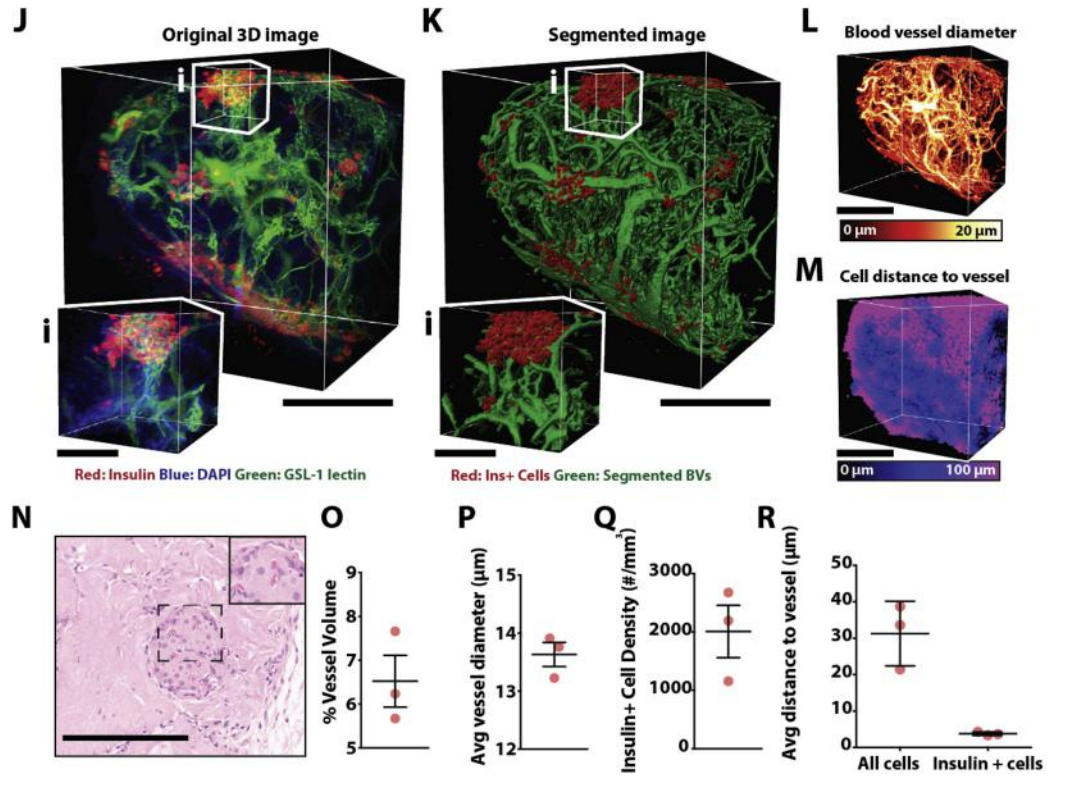


*(caption on next page)*

**Fig. 5. 3-D vascular features of pseudo-islets and islet modules at day 21.** CLARITY-processed grafts of **A)** pseudo-islets and **J)** islet modules at day 21 stained with DAPI (blue, nuclei), GSL-1 lectin (green, vessels) and insulin (red). **B, K**) Insulin$^+$ cells and blood vessels were segmented to create a binary image. Insets **(i)** highlight a higher magnification volume of insulin$^+$ cells integrating with the perfusable vasculature. Maximum intensity projection images of **C)** pseudo-islets and **L)** islet modules pseudo-coloured to see differences in the diameters of blood vessels. Maximum intensity projection images of **D)** pseudo-islets and **M)** islet modules pseudo-coloured to see the distances of cells to perfusable vessels. **E, N)** Distribution of β-cells and the associated vasculature visualized using Hematoxylin & Eosin staining of pseudo-islets and islet modules, respectively. Arrowheads denote β-cells within pseudo-islets. Insets show higher magnification images of β-cells closely associated with vessels. Scale bars = 200 μm. **F, O)** % vessel volumes, **G, P)** average vessel diameters and **H, Q)** insulin$^+$ cell densities of pseudo-islets and islet modules, respectively at day 21. **I, R)** The average distance of "all cells" or insulin$^+$ cells to vessels of pseudo-islets and islet modules, respectively. The average distance of insulin$^+$ cells in both groups was within 5 μm of a perfusable vessel. n = 3 for both groups. Averages ± SEM. Scale bars = 500 μm. Scale bars of insets = 50 μm. (For interpretation of the references to colour in this figure legend, the reader is referred to the Web version of this article.)

transplantation into the subcutaneous space. Despite its limited utility, Matrigel™ has been used to subcutaneously deliver pseudo-islets and achieve some effect on glucose levels in some animals [43]. However, more clinically relevant scaffolds, such as collagen are important for translation.

In this study, size-controlled tuneable pseudo-islets were engineered using endothelialized collagen rods (Fig. 1), to form all-in-one islet constructs that were functionally comparable to native islets in vitro (Fig. 3), survived engraftment in the subcutaneous space (Fig. 4A, Supplementary Fig. 12C), and were retrievable (Supplementary Fig. 9A). Alternative methods fabricating pseudo-islets rely on cell-driven aggregation methods [41,44], which can be difficult to manipulate and can result in cell loss [45], precluding the advantages of digesting islets to form pseudo-islets.

Digesting pancreatic islets into a single cell suspension enabled manipulation of the cellular composition, cellular density, and size of pseudo-islets (Fig. 2C) - something not possible with native islets or other pseudo-islet approaches. The ability to enrich or remove specific cell populations is of interest, as it would allow pseudo-islets to be designed to exploit the reported difference in insulin secretion activity found in the heterogeneous β-cell population [46,47]. The possible variations in therapeutic efficacy of pseudo-islets formed with only particular β-cell sub-populations (or reprogrammed β-cells [18]) could guide the design of a more therapeutic islet construct. While some non-beta cells are still required [48], it is useful to recognize that this control of composition would allow the removal of minimally therapeutic but equivalently oxygen-consuming cells, thus reducing the design limiting-oxygen demand [37] of the transplant tissue.

Furthermore, the ability to control the size of the pseudo-islets is important since pancreatic islet size affects the development of a hypoxic core [13] and transplantation efficacy [12]. By seeding HUVEC on the surface, pseudo-islets contracted and remodelled over time in culture (Fig. 2D and E – blue lines). Other pseudo-islet approaches rely on changing the initial number of single islet cells to control the size of their pseudo-islets [17,49,50], while here the initial size of the collagen gel rods [51], cell composition, and culture time determines the size of the pseudo-islets (Fig. 2D and Supplementary Fig. 5A). We did not explicitly test the effect that pseudo-islet size has on therapeutic efficacy, but pseudo-islets can be made using smaller-diameter collagen gel rods [51] or embedding additional cells such as adMSC to yield significantly smaller constructs (Fig. 4D).

### 4.2. Subcutaneously transplanted pseudo-islets rectify normoglycemia

Pseudo-islets were capable of engrafting and returning STZ-induced diabetic mice to normoglycemia when subcutaneously transplanted (Fig. 4A). Since native free islets did not show any therapeutic effect (Fig. 4A, red line), we attributed the return to normoglycemia in the pseudo-islet group to the enhanced ability to engraft in the subcutaneous space due to the endothelialized collagen scaffold (Fig. 4, blue solid line). Islet modules also returned animals to normoglycemia (Fig. 4 – blue dotted line), but this return was delayed compared to pseudo-islets, possibly because embedding a single cell suspension is easier than embedding whole islets. Native islet modules were cultured for 4 days prior to transplantation (to be consistent with pseudo-islets), which may have contributed to their reduced therapeutic efficacy compared to previous studies where they were only cultured overnight before transplantation [6]. It should be noted that although we transplanted an equivalent number of islet cells, the volume of pseudo-islet grafts was smaller than native islet module grafts (70 μL vs. 100 μL), which may also have contributed to this faster response.

AdMSC were incorporated into some groups of pseudo-islets, since they have been reported to be beneficial for islet function and engraftment [20]. However, in a previous study the addition of adMSC was detrimental to the therapeutic efficacy of the islet modules due to the competition for nutrients and oxygen at early time points [6]. Therefore, the embedded adMSC density was reduced by ten-fold in the pseudo-islets studied here to minimize this competition and recover the potential regenerative properties of these cells. Indeed, pseudo-islets + adMSC showed an increased amount of insulin secreted when stimulated with glucose in vitro, compared to native islets and pseudo-islets without adMSC (Fig. 2D). However in vivo, the inclusion of adMSC did not promote significantly more vasculature (CD31$^+$ vessels) or increase the percentage of insulin$^+$ cells when compared to pseudo-islets without adMSC at day 21 (Supplementary Figs. 12B and C). Adding adMSC into the pseudo-islets improved their therapeutic efficacy by reducing the average time it took to become normoglycemic (Supplementary Figs. 9A and B – green line). Pseudo-islets with adMSC were significantly smaller and showed an increased insulin secretion relative to pseudo-islets (Fig. 2D), which may have contributed to the rapid return to normoglycemia. Interestingly, the addition of adMSC (even with a ten-fold reduction in number compared to previous work [6]) was still detrimental to islet function when included within native islet modules (Supplementary Fig. 10). Previously, it has been shown that islet modules with adMSC were well-vascularized [6]. We presume that islet deaggregation results in a different microenvironment within the pseudo-islets, which caused pseudo-islet-embedded adMSC to secrete different paracrine factors [52] than those embedded within native islet modules.

### 4.3. Revascularization of pseudo-islets in the subcutaneous space

β-cells must be closely associated with perfusable vessels to reliably respond to fluctuations in blood glucose and maintain glucose homeostasis [53]. Previous studies have determined that the majority of β-cells are adjacent to endothelial cells [54] and after staining the whole-implants for insulin, the average distance of an insulin$^+$ β-cell was within 5 μm of a perfusable vessel (Fig. 5A, I). Although pseudo-islet fabrication destroys the intrinsic vasculature network, this vasculature architecture was regenerated upon subcutaneous transplantation (Fig. 5A inset) – a feature not previously shown. We expect that this revascularization explains the ability of these pseudo-islets to regulate blood glucose and respond to a glucose bolus (Fig. 4A, C). This type of vascular integration was also observed with islet modules in the subcutaneous space (Fig. 5J), and was similar to that seen in the native pancreas (Supplementary Fig. 14A).

The majority of insulin$^+$ cells were distributed close to the periphery of the implants at day 21 (Fig. 5A, J), which was also confirmed by histology (Supplementary Fig. 15). Since the modular tissue engineering approach drives angiogenesis by forming chimeric

vasculature with the host at early time points [55,56], the greatest number of vessels are present at the periphery of the implant during initial vascularization (days 0–7). Because CLARITY-processing is done at experimental endpoints, we cannot determine whether individual islet cells within the pseudo-islet grafts migrated towards the tissue periphery, or if cells found within the core of the graft did not survive the revascularization process. Nevertheless, this type of revascularization for pseudo-islets has not been previously shown in the subcutaneous space. Future studies could investigate the revascularization dynamics by using intra-vital imaging with fluorescently labelled islets [57] or specific β-cell subsets to track changes in the distribution of islet cells within the graft over time.

## 5. Conclusion

In this study, size-controlled and tuneable pseudo-islets were fabricated by embedding deaggregated pancreatic islets into endothelialized collagen rods. These pseudo-islets had comparable insulin secretion activity to native islets and returned streptozotocin-induced diabetic SCID/bg mice to normoglycemia when subcutaneously transplanted. Using histology and whole-implant imaging, it was confirmed that subcutaneously transplanted pseudo-islets regenerated the intrinsic vascular architecture and integrated with the host – a feature not seen with other pseudo-islet approaches. Finally, insulin$^+$ β-cells within subcutaneously transplanted pseudo-islet grafts were found within 5 μm from a perfusable host vessel, consistent with pancreatic islets within the native pancreas. By tuning cell composition and the intrinsic scaffold properties, this pseudo-islet platform can allow for a “bottom-up” approach to design a more therapeutic islet construct that can survive engraftment in the subcutaneous space.

## Summary

In this study we show that engineered size-controlled pseudo-islet collagen constructs are superior to native islets when implanted underneath the skin of diabetic mice. Pseudo-islets integrated with the host's vasculature and regenerated their intrinsic vascular architecture as confirmed using 3D imaging. This work highlights a platform that provides a greater control over native islets to enable enhanced implants for islet transplantation.

## Author contributions

A.E.V., S.M.K., B.R.K., S.K., and M.V.S. conceived the study. A.E.V., S.M.K., S.K., B.R.K., S.W., and A.M. performed the experiments for the manuscript. A.E.V., S.M.K., S.K., S.W., and B.R.K. analyzed the data for the manuscript. A.E.V., and M.V.S. wrote the manuscript. All of the authors edited and provided feedback for the manuscript.

## Declaration of interests

The authors declare no competing interests.

## Acknowledgements

We would like to thank Chuen Lo for his help and expertise with animal surgeries and islet isolations. In addition, we would like to thank Tairan Qin and Herbert Gaisano for help with the perifusion experiments. In addition, we would like to thank Hima Gohil and Mike Wheeler for their help with oxygen consumption rate experiments. This work was supported by CIHR (341676) and JDRF (3-SRA-2016-253-S-B). A.E.V. was supported by scholarships from the Province of Ontario and the Jennifer Dorrington Award. A.E.V. and S.Ke. received scholarships from the Banting and Best Diabetes Centre. B.R.K. was supported by scholarships and fellowships including NSERC PGS-D, RBC Graduate Fellowship the Wildcat foundation and the Donnelly Centre.

## Appendix A. Supplementary data

Supplementary data to this article can be found online at https://doi.org/10.1016/j.biomaterials.2019.119710.

## References

[1] D.L. Eizirik, M.L. Colli, F. Ortis, The role of inflammation in insulitis and β-cell loss in type 1 diabetes, Nat. Rev. Endocrinol. 5 (2009) 219–226, https://doi.org/10.1038/nrendo.2009.21.
[2] A.M.J. Shapiro, J.R.T. Lakey, E.A. Ryan, G.S. Korbutt, E. Toth, G.L. Warnock, et al., Islet transplantation in seven patients with type 1 diabetes mellitus using a glucocorticoid-free immunosuppressive regimen, N. Engl. J. Med. 343 (2000) 230–238, https://doi.org/10.1056/NEJM200007273430401.
[3] N.R. Barshes, Inflammation-mediated dysfunction and apoptosis in pancreatic islet transplantation: implications for intrahepatic grafts, J. Leukoc. Biol. 77 (2005) 587–597, https://doi.org/10.1189/jlb.1104649.
[4] A.M.J. Shapiro, Strategies toward single-donor islets of Langerhans transplantation, Curr. Opin. Organ Transplant. 16 (2011) 627–631, https://doi.org/10.1097/MOT.0b013e32834cfb84.
[5] A.R. Pepper, B. Gala-Lopez, R. Pawlick, S. Merani, T. Kin, A.M.J. Shapiro, A prevascularized subcutaneous device-less site for islet and cellular transplantation, Nat. Biotechnol. 33 (2015) 518–523, https://doi.org/10.1038/nbt.3211.
[6] A.E. Vlahos, N. Cober, M.V. Sefton, Modular tissue engineering for the vascularization of subcutaneously transplanted pancreatic islets, Proc. Natl. Acad. Sci. 114 (2017) 9337–9342, https://doi.org/10.1073/pnas.1619216114.
[7] J.D. Weaver, D.M. Headen, J. Aquart, C.T. Johnson, L.D. Shea, H. Shirwan, et al., Vasculogenic hydrogel enhances islet survival, engraftment, and function in leading extrahepatic sites, Science Advances 3 (2017) e1700184, , https://doi.org/10.1126/sciadv.1700184.
[8] R. Mahou, D.K.Y. Zhang, A.E. Vlahos, M.V. Sefton, Injectable and inherently vascularizing semi-interpenetrating polymer network for delivering cells to the subcutaneous space, Biomaterials 131 (2017) 27–35, https://doi.org/10.1016/j.biomaterials.2017.03.032.
[9] C.H. Stephens, K.S. Orr, A.J. Acton, S.A. Tersey, R.G. Mirmira, R.V. Considine, et al., In-situ type I oligomeric collagen macroencapsulation promotes islet longevity and function in vitro and in vivo, Am. J. Physiol. Endocrinol. Metab. 19 (2018) 1523, https://doi.org/10.1152/ajpendo.00073.2018.
[10] A.R. Pepper, B. Gala-Lopez, O. Ziff, A.M.J. Shapiro, Revascularization of transplanted pancreatic islets and role of the transplantation site, Clin. Dev. Immunol. 2013 (2013) 1–13, https://doi.org/10.1155/2013/352315.
[11] L. Jansson, P.O. Carlsson, Graft vascular function after transplantation of pancreatic islets, Diabetologia 45 (2002) 749–763, https://doi.org/10.1007/s00125-002-0827-4.
[12] D. Zorzi, T. Phan, M. Sequi, Y. Lin, D.H. Freeman, L. Cicalese, et al., Impact of islet size on pancreatic islet transplantation and potential interventions to improve outcome, Cell Transplant. 24 (2015) 11–23, https://doi.org/10.3727/096368913X673469.
[13] R. Lehmann, R.A. Zuellig, P. Kugelmeier, P.B. Baenninger, W. Moritz, A. Perren, et al., Superiority of small islets in human islet transplantation, Diabetes 56 (2007) 594–603, https://doi.org/10.2337/db06-0779.
[14] K.I. Rother, D.M. Harlan, Challenges facing islet transplantation for the treatment of type 1 diabetes mellitus, J. Clin. Investig. 114 (2004) 877–883, https://doi.org/10.1172/JCI200423235.
[15] N. Kojima, In vitro reconstitution of pancreatic islets, Organogenesis 10 (2014) 225–230, https://doi.org/10.4161/org.28351.
[16] Y. Takahashi, K. Sekine, T. Kin, T. Takebe, H. Taniguchi, Self-condensation culture enables vascularization of tissue fragments for efficient therapeutic transplantation, Cell Rep. 23 (2018) 1620–1629, https://doi.org/10.1016/j.celrep.2018.03.123.
[17] Y. Yu, A. Gamble, R. Pawlick, A.R. Pepper, B. Salama, D. Toms, et al., Bioengineered Human Pseudoislets Form Efficiently from Donated Tissue, Compare Favourably with Native Islets in Vitro and Restore Normoglycaemia in Mice, (2018), pp. 1–14, https://doi.org/10.1007/s00125-018-4672-5.
[18] K. Furuyama, S. Chera, L. Gurp, D. Oropeza, L. Ghila, N. Damond, et al., Diabetes relief in mice by glucose-sensing insulin-secreting human α-cells, Nature (2019) 1–30, https://doi.org/10.1038/s41586-019-0942-8.
[19] S. Vériter, P. Gianello, D. Dufrane, Bioengineered sites for islet cell transplantation, Curr. Diabetes Rep. 13 (2013) 745–755, https://doi.org/10.1007/s11892-013-0412-x.
[20] A. Gamble, R. Pawlick, A.R. Pepper, A. Bruni, A. Adesida, P.A. Senior, et al., Improved islet recovery and efficacy through co-culture and co-transplantation of islets with human adipose-derived mesenchymal stem cells, PLoS One 13 (2018), https://doi.org/10.1371/journal.pone.0206449 e0206449–17.
[21] P. Quaranta, S. Antonini, S. Spiga, B. Mazzanti, M. Curcio, G. Mulas, et al., Co-transplantation of endothelial progenitor cells and pancreatic islets to induce long-lasting normoglycemia in streptozotocin-treated diabetic rats, PLoS One 9 (2014), https://doi.org/10.1371/journal.pone.0094783 e94783–13.
[22] A.P. McGuigan, M.V. Sefton, Vascularized organoid engineered by modular assembly enables blood perfusion, Proc. Natl. Acad. Sci. 103 (2006) 11461–11466, https://doi.org/10.1073/pnas.0602740103.
[23] S. Bolte, F.P. Cordelières, A guided tour into subcellular colocalization analysis in light microscopy, J. Microsc. 224 (2006) 213–232, https://doi.org/10.1111/j.1365-2818.2006.01706.x.
[24] T. Qin, T. Liang, D. Zhu, Y. Kang, L. Xie, S. Dolai, et al., Munc18b increases insulin

granule fusion, restoring deficient insulin secretion in type-2 diabetes human and goto-kakizaki rat islets with improvement in glucose homeostasis, EBioMedicine 16 (2017) 262–274, https://doi.org/10.1016/j.ebiom.2017.01.030.
[25] J.H.R. Kenty, D.A. Melton, Testing pancreatic islet function at the single cell level by calcium influx with associated marker expression, PLoS One 10 (2015), https://doi.org/10.1371/journal.pone.0122044 e0122044–17.
[26] S. Sindhwani, A.M. Syed, S. Wilhelm, D.R. Glancy, Y.Y. Chen, M. Dobosz, et al., Three-dimensional optical mapping of nanoparticle distribution in intact tissues, ACS Nano 10 (2016) 5468–5478, https://doi.org/10.1021/acsnano.6b01879.
[27] R. Tomer, L. Ye, B. Hsueh, K. Deisseroth, Advanced CLARITY for rapid and high-resolution imaging of intact tissues, Nat. Protoc. 9 (2014) 1682–1697, https://doi.org/10.1038/nprot.2014.123.
[28] C. Sommer, C. Straehle, U. Kothe, F.A. Hamprecht, Ilastik: interactive learning and segmentation toolkit, 2011 IEEE International Symposium on Biomedical Imaging: from Nano to Macro, 2011, pp. 230–233, , https://doi.org/10.1109/ISBI.2011.5872394.
[29] P.A. Games, J.F. Howell, Pairwise multiple comparison procedures with unequal N's and/or variances: a Monte Carlo study, J. Educ. Stat. 1 (1976) 113–125, https://doi.org/10.2307/1164979?ref=search-gateway:89358de9b92abc94d830465ba7295f60.
[30] R.N. Wang, L. Rosenberg, Maintenance of beta-cell function and survival following islet isolation requires re-establishment of the islet-matrix relationship, J. Endocrinol. 163 (1999) 181–190.
[31] A. Pisania, G.C. Weir, J.J. O'Neil, A. Omer, V. Tchipashvili, J. Lei, et al., Quantitative analysis of cell composition and purity of human pancreatic islet preparations, Lab. Investig. 90 (2010) 1661–1675, https://doi.org/10.1038/labinvest.2010.124.
[32] Y. Wang, K.K. Danielson, A. Ropski, T. Harvat, B. Barbaro, D. Paushter, et al., Systematic analysis of donor and isolation factor's impact on human islet yield and size distribution, Cell Transplant. 22 (2013) 2323–2333, https://doi.org/10.3727/096368912X662417.
[33] O. Cabrera, D.M. Berman, N.S. Kenyon, C. Ricordi, P.-O. Berggren, A. Caicedo, The unique cytoarchitecture of human pancreatic islets has implications for islet cell function, Proc. Natl. Acad. Sci. 103 (2006) 2334–2339, https://doi.org/10.1073/pnas.0510790103.
[34] D. Bosco, D.G. Rouiller, P.A. Halban, Differential expression of E-cadherin at the surface of rat -cells as a marker of functional heterogeneity, J. Endocrinol. 194 (2007) 21–29, https://doi.org/10.1677/JOE-06-0169.
[35] D.G. Pipeleers, P.A. IN'T VELD, M. Van de Winkel, E. MAES, F.C. SCHUIT, W. GEPTS, A new in vitro model for the study of pancreatic A and B cells, Endocrinology 117 (1985) 806–816, https://doi.org/10.1210/endo-117-3-806.
[36] C. Fraker, M.R. Timmins, R.D. Guarino, P.D. Haaland, H. Ichii, D. Molano, et al., The use of the BD oxygen biosensor system to assess isolated human islets of langerhans: oxygen consumption as a potential measure of islet potency, Cell Transplant. 15 (2006) 745–758.
[37] K.K. Papas, C.K. Colton, R.A. Nelson, P.R. Rozak, E.S. Avgoustiniatos, W.E. Scott, et al., Human islet oxygen consumption rate and DNA measurements predict diabetes reversal in nude mice, Am. J. Transplant. 7 (2007) 707–713, https://doi.org/10.1111/j.1600-6143.2006.01655.x.
[38] A. Kerby, E.S. Jones, P.M. Jones, A.J. King, Co-transplantation of islets with mesenchymal stem cells in microcapsules demonstrates graft outcome can be improved in an isolated-graft model of islet transplantation in mice, Journal of Cytotherapy 15 (2013) 192–200, https://doi.org/10.1016/j.jcyt.2012.10.018.
[39] A.R. Pepper, C. Gall, D.M. Mazzuca, C.W.J. Melling, D.J.G. White, Diabetic rats and mice are resistant to porcine and human insulin: flawed experimental models for testing islet xenografts, Xenotransplantation 16 (2009) 502–510, https://doi.org/10.1111/j.1399-3089.2009.00548.x.
[40] P. Fraisl, J. Aragonés, P. Carmeliet, Inhibition of oxygen sensors as a therapeutic strategy for ischaemic and inflammatory disease, Nat. Rev. Drug Discov. 8 (2009) 139–152, https://doi.org/10.1038/nrd2761.
[41] E.S. O'Sullivan, A. Vegas, D.G. Anderson, G.C. Weir, Islets transplanted in immunoisolation devices: a review of the progress and the challenges that remain, Endocr. Rev. 32 (2011) 827–844, https://doi.org/10.1210/er.2010-0026.
[42] C. Wittig, M.W. Laschke, C. Scheuer, M.D. Menger, Incorporation of bone marrow cells in pancreatic pseudoislets improves posttransplant vascularization and endocrine function, PLoS One 8 (2013), https://doi.org/10.1371/journal.pone.0069975 e69975–12.
[43] S. Pathak, S. Regmi, B. Gupta, T.T. Pham, C.S. Yong, J.O. Kim, et al., Engineered islet cell clusters transplanted into subcutaneous space are superior to pancreatic islets in diabetes, FASEB J. 31 (2017) 5111–5121, https://doi.org/10.1096/fj.201700490R.
[44] P.A. Halban, S.L. Powers, K.L. George, S. Bonner-Weir, Spontaneous reassociation of dispersed adult rat pancreatic islet cells into aggregates with three-dimensional architecture typical of native islets, Diabetes 36 (1987) 783–790.
[45] H. Callewaert, C. Gysemans, A.K. Cardozo, M. Elsner, M. Tiedge, D.L. Eizirik, et al., Cell loss during pseudoislet formation hampers profound improvements in islet lentiviral transduction efficacy for transplantation purposes, Cell Transplant. 16 (2007) 527–537.
[46] R.K.P. Benninger, D.J. Hodson, New understanding of β-cell heterogeneity and in situ islet function, Diabetes 67 (2018) 537–547, https://doi.org/10.2337/dbi17-0040.
[47] C. Dorrell, J. Schug, P.S. Canaday, H.A. Russ, B.D. Tarlow, M.T. Grompe, et al., Human islets contain four distinct subtypes of β cells, Nature Publishing Group. 7 (1AD) 1–9. doi:10.1038/ncomms11756.
[48] K. Hamaguchi, N. Utsunomiya, R.T. Experimental, Cellular interaction between mouse pancreatic α-cell and β-cell lines: possible contact-dependent inhibition of insulin secretion, Journals.Sagepub.com . 228 (2003) 1227–1233, https://doi.org/10.1177/153537020322801020 2016.
[49] K. Ramachandran, S.J. Williams, H.-H. Huang, L. Novikova, L. Stehno-Bittel, Engineering islets for improved performance by optimized reaggregation in a micromold, Tissue Eng. A 19 (2013) 604–612, https://doi.org/10.1089/ten.tea.2012.0553.
[50] E.S. O'Sullivan, A.S. Johnson, A. Omer, J. Hollister-Lock, S. Bonner-Weir, C.K. Colton, et al., Rat islet cell aggregates are superior to islets for transplantation in microcapsules, Diabetologia 53 (2010) 937–945, https://doi.org/10.1007/s00125-009-1653-8.
[51] B.M. Leung, M.V. Sefton, A modular approach to cardiac tissue engineering, Tissue Eng. A 16 (2010) 3207–3218, https://doi.org/10.1089/ten.tea.2009.0746.
[52] G.D. Kusuma, J. Carthew, R. Lim, J.E. Frith, Effect of the microenvironment on mesenchymal stem cell paracrine signaling: opportunities to engineer the therapeutic effect, Stem Cells Dev. 26 (2017) 617–631, https://doi.org/10.1089/scd.2016.0349.
[53] N. Ballian, F.C. Brunicardi, Islet vasculature as a regulator of endocrine pancreas function, World J. Surg. 31 (2007) 705–714, https://doi.org/10.1007/s00268-006-0719-8.
[54] S. Bonner-Weir, Morphological evidence for pancreatic polarity of β-cell within islets of langerhans, Diabetes 37 (1988) 616–621, https://doi.org/10.2337/diab.37.5.616.
[55] M.D. Chamberlain, R. Gupta, M.V. Sefton, Bone marrow-derived mesenchymal stromal cells enhance chimeric vessel development driven by endothelial cell-coated microtissues, Tissue Eng. A 18 (2012) 285–294, https://doi.org/10.1089/ten.tea.2011.0393.
[56] G.C. Lam, M.V. Sefton, Tuning graft- and host-derived vascularization in modular tissue constructs: a potential role of HIF1 activation, Tissue Eng. A (2014), https://doi.org/10.1089/ten.tea.2014.0315 141107113828001.
[57] L. Gurp, C.J.M. Loomans, P.P. Krieken, G. Dharmadhikari, E. Jansen, F.C.A.S. Ringnalda, et al., Sequential intravital imaging reveals in vivo dynamics of pancreatic tissue transplanted under the kidney capsule in mice, Diabetologia (2016) 1–6, https://doi.org/10.1007/s00125-016-4049-6.